

Ibn Al-Haitham Journal for Pure and Applied Sciences

Journal homepage: jih.uobaghdad.edu.iq PISSN: 1609-4042, EISSN: 2521-3407 IHJPAS. 2025, 38(4)



Commercial Graphite Flakes as an Adsorbent of Janus Green Dye from Aqueous Solution: Adsorption Kinetics and Isotherms Study

Nagham H. Abood^{1,2} □ ✓ and Sundus H. Merza^{2*} □ ✓

¹Department of Applied Science, Applied Chemistry, University of Technology, Baghdad, Iraq.

²Department of Chemistry, College of Education for Pure Science (Ibn Al-Haitham), University of Baghdad, Baghdad, Iraq.

*Corresponding Author.

Received: 13 March 2025 Accepted: 21 July 2025 Published: 20 October 2025

doi.org/10.30526/38.4.4140

Abstract

Commercial graphite (CGT) powder was used as an adsorbent surface for cationic dye, Janus green (JG), from aqueous solutions. This study aims to highlight the practical significance of using inexpensive CGT as an efficient adsorbent for the removal of JG dye from industrial wastewater. CGT was characterized by Fourier transform infrared spectroscopy, scanning electron microscopy, and X-ray diffraction. The adsorption process was investigated by examining parameters like the weight of the adsorbent, contact time, and temperature. Pseudo-second-order kinetic (PSO), pseudo-first-order, and intraparticle diffusion were used for analyzing the kinetic data. JG dye's adsorption kinetics fit the PSO kinetic model well (R^2 = 0.999). Furthermore, the thermodynamic functions such as entropy (ΔS^*) , enthalpy (ΔH^*) , and Gibbs free energy (ΔG^*) were evaluated. The positive value of (ΔH^*) confirms that the adsorption process is endothermic. Also, the positive value of ΔS^* suggests an increase in randomness at the solid-liquid interface during dye adsorption, and non-spontaneous as evidenced by positive ΔG^* values of 76.686, 76.130, 75.574, and 75.018 kJ/mol at different temperatures. Two segment-linear plots have been used to describe the intraparticle diffusion analysis of JG adsorption onto CGT, and the plot does not meet the origin point, indicating that the intraparticle diffusion was not the only controlling step. Based on the calculated value of $\Delta H^*= 92.701$ kJ/mol, which means that the adsorption is a chemical type. Langmuir, Freundlich, and Temkin isotherms were studied for their isothermal behavior. Also, the equilibrium state is attained in 45 minutes. At 318.15 K, the maximum removal percentage of JG achieved is 99.96%, indicating that the graphite surface is suitable as an adsorbent surface for removing JG dye in the temperature range studied.

Keywords:Fourier transform infrared spectroscopy, Graphite, Temkin isotherm, Thermodinamics, X-ray diffraction.

1. Introduction

Water is crucial for every living organism, covering 71% of the Earth's surface. Consequently, water pollution is a significant environmental issue, particularly due to its impact on aquatic biodiversity by obstructing light penetration (1). Various industries extensively use synthetic dyes, which are essential contributors to water pollution. These dyes

manipulate the physical and chemical attributes of water, including its characteristics and quality (2). In addition to these changes, the complex molecular structures of the dyes can pose potential risks, including toxicity to human health, wildlife, and ecosystems (3). A variety of physicochemical and biological techniques (4) have been employed to eliminate dyes from wastewater. However, many of these techniques are costly, particularly when applied to large-scale wastewater treatment. Therefore, adsorption technology has been used as an essential method for treating water pollution due to its low cost and the availability of various natural materials that can serve as effective adsorbent surfaces, including a range of organic, inorganic substances, and calcium-cellulose-based materials (5). Graphite (GT) refers to a pure crystalline substance composed of carbon atoms arranged in trigonal units. These atoms undergo sp² hybridization, resulting in a structure with minimal impurities (6). Graphite's unique properties arise from two types of bonds: σ-bonds, which form between adjacent carbon atoms, and π -bonds, which are delocalized above and below the carbon layers (7). The carbon atoms in GT are arranged in hexagonal or rhombohedral unit cells, forming a layered crystal structure. Each atomic layer of graphite is called graphene (8). Furthermore, GT exhibits high electrical and thermal conductivity and is broadly used in many applications in industries (9). Due to its availability, water-insolubility, and natural non-toxicity, the graphite GT is considered a promising option for real-world wastewater treatment facilities, mainly in the textile industry. To the best of our knowledge, GT has not been extensively investigated as an adsorbent for dyes; however, a few studies have emphasized its potential in removing various pollutants, such as aromatic compounds and ions like fluoride and ammonium (10). The Janus Green (JG) is a dark green cationic dye that remains unaffected by pH changes. It is used in histology applications to stain cellular components and microorganisms (11). This study aims to highlight the practical significance of using inexpensive commercial graphite (CGT) as an efficient adsorbent for the removal of JG dye from industrial wastewater.

2. Materials and Methods

A Labtech shaking water bath and UV-visible spectrophotometer (Shimadzu UV-1800) were used to study the adsorption process. Sartorius balance (L420 B ± 0.0001) and Hettich centrifuge (EBA-20) were also used. JG dye (133) with the empirical formula $C_{30}H_{31}ClN_6$ (M.W= 511.06 g/mol, pH=7, melting point > 200C°) was used. The CGT was used as the adsorbent without prior treatment. A German sieve with a 75-micrometer mesh size was used to sift the CGT. The structural properties of CGT were examined using CuK α radiation in an X-ray diffractometer (6000/ Shimadzu-Japan) along with energy dispersive X-ray spectroscopy (EDXS) and scanning electron microscopy (Zeiss). Chemical structure information was obtained using a Fourier transform infrared (FT-IR) spectrophotometer (Shimadzu-8400S, Japan) in the 400 to 4000 cm⁻¹ range.

2.1. Determination of maximum absorption of Janus green dye

UV-visible spectrum of JG dye, measured over the range 90-1100 nm, is depicted in **Figure** 1. The highest absorbance (λ_{max}) for JG dye was found at 611 nm. This value was used in all quantitative assessments conducted in this study.

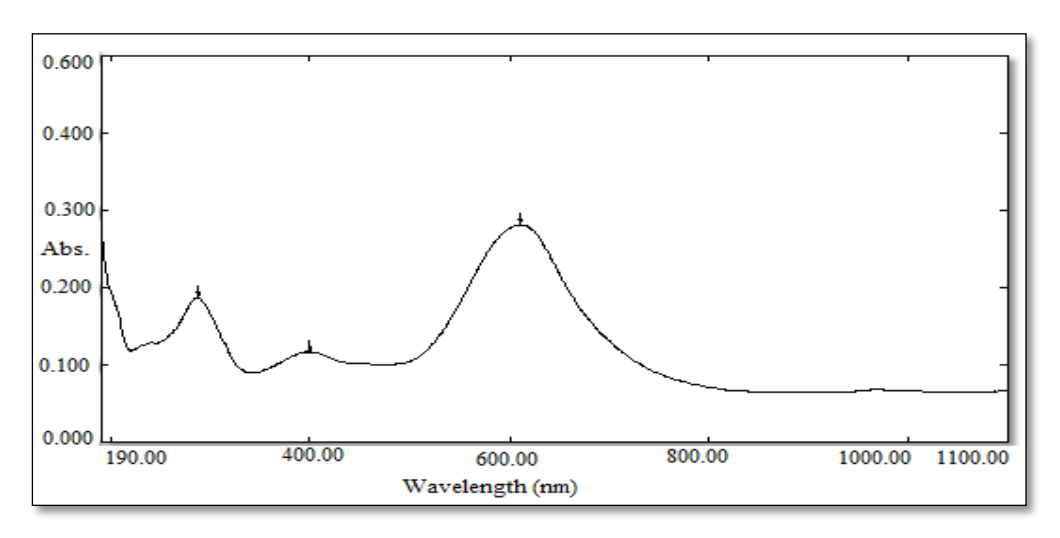


Figure 1. Maximum absorption peak of JG dye.

2.2. Determination of the calibration curve for the commercial graphite adsorbent

A series of solutions with varying concentrations ranging from 3 to 42 mg/L in increments of 3 mg/L was prepared to determine the calibration curve for the JG dye. The absorbance values of the dye solutions were measured and plotted against the concentration according to Beer-Lambert's law, as shown in **Figure 2**.

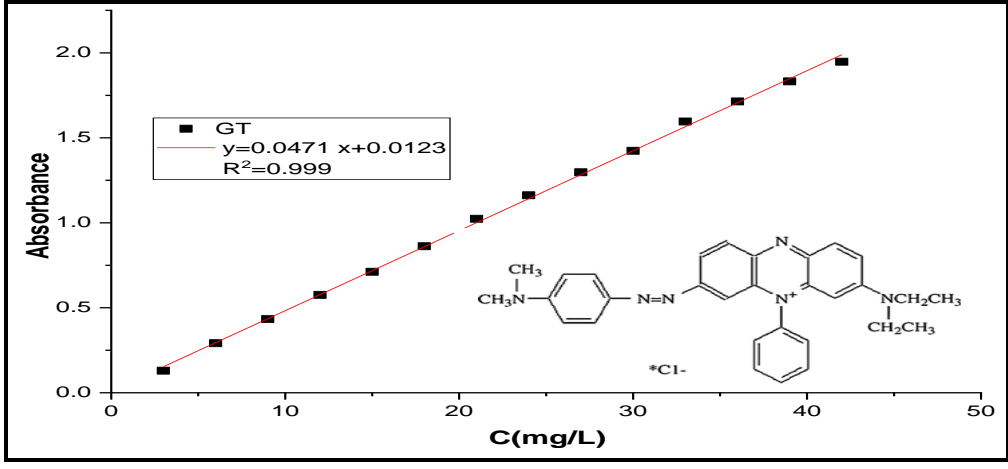


Figure 2. JG dye standard calibration plot.

2.3. Adsorption experiments

Adsorption experiments were performed by agitating varying weights of CGT adsorbent with 10 mL of (42 mg/L) neutral aqueous solution of JG dye at pH 7 and a temperature of 25 ± 0.5 °C. The solutions were transferred to stoppered bottles placed in a controlled shaking water bath at 150 rpm for 60 minutes. Upon completion of the period, the samples were centrifuged for 10 minutes at 4000 rpm. The absorbance of the supernatant was measured using an ultraviolet-visible spectrophotometer at λ_{max} = 611 nm. The percentage of adsorption removal (R%) was calculated using the formula below (12, 13).

$$R\% = \frac{(C_{\circ} - C_t)}{C_{\circ}} \times 100 \tag{1}$$

Where C_0 (mg/L) and C_t (mg/L) signify the initial concentration and the concentration of the solution at the time, respectively, to analyze the influence of varying temperatures (T) on the kinetic behavior of the removal process, the equilibrium time was determined by mixing the optimum weight of CGT (0.15 g) with 10 mL of dye solution. The amount of JG adsorbed onto CGT was calculated using the **Equation 2** at different time intervals (5–180 min) (14,15):

$$q_t = \frac{(C_\circ - C_t)V}{m} \tag{2}$$

Where q_t (mg/g) represents the amount of adsorbed material at time t. C_{\circ} (mg/L) and C_t (mg/L) denote the initial concentration of the solution and the concentration at time t, respectively. m (g) is the weight of the adsorbent, and V (mL) is the volume of the dye solution. The isothermal behavior of the adsorption process was studied using 10 mL of dye solutions with concentrations varying from 35 to 80 mg/L under optimum conditions at different T. The equilibrium quantity of JG adsorbed, q_e (mg/g), was determined according to **Equation 2**, assuming $q_t = q_e$ and $C_t = C_e$.

3. Results

3.1. Identification of commercial graphite

3.1.1. The X- ray diffraction analysis

The X-ray diffractogram (XRD) of CGT allows for the evaluation of its structural and crystallographic properties, as shown in **Figure 3**. Additionally, the crystallite size of CGT along the c-direction (t_c) or its thickness was computed to be 26.085 nm using the classical Scherrer equation (**Equation 3**):

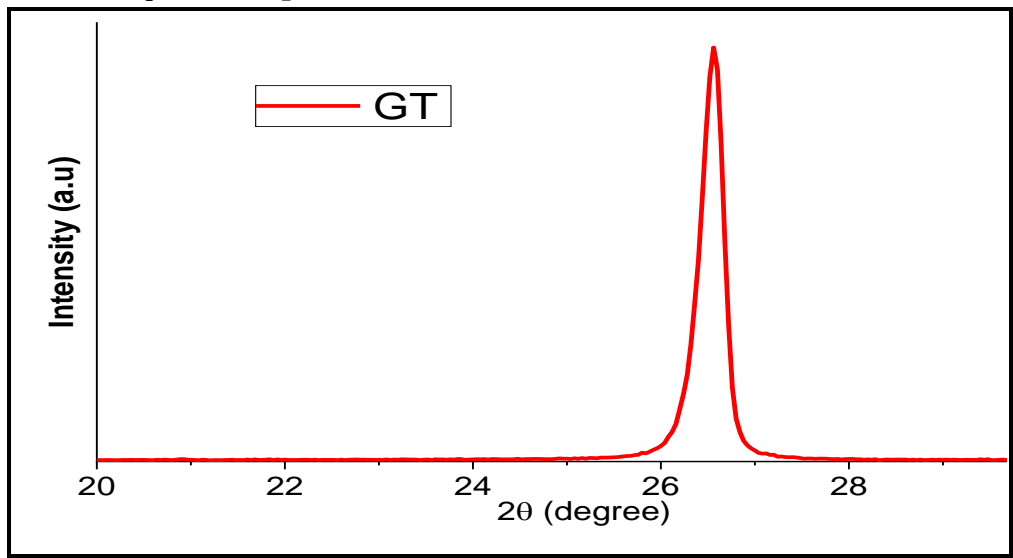


Figure 3. XRD pattern of CGT.

$$t_c = \frac{0.94\lambda}{\beta_D \cos \theta} \tag{3}$$

Where θ is the angle of incidence in radians, and β_D is the full width at half maximum (FWHM) (16). The average number of layers (n) is given by the **Equation 4**.

$$\frac{t_c}{d_{002}} + 1$$
(4)

3.1.2. The SEM and EDX

The morphology of the CGT adsorbent before adsorption of JG dye and after adsorption was examined utilizing SEM, as shown in **Figure 4 A** and **B**. **Figure 4 C** and **D** illustrate the atomic content of the CGT adsorbent before and after adsorption of JG dye as determined by EDXS.

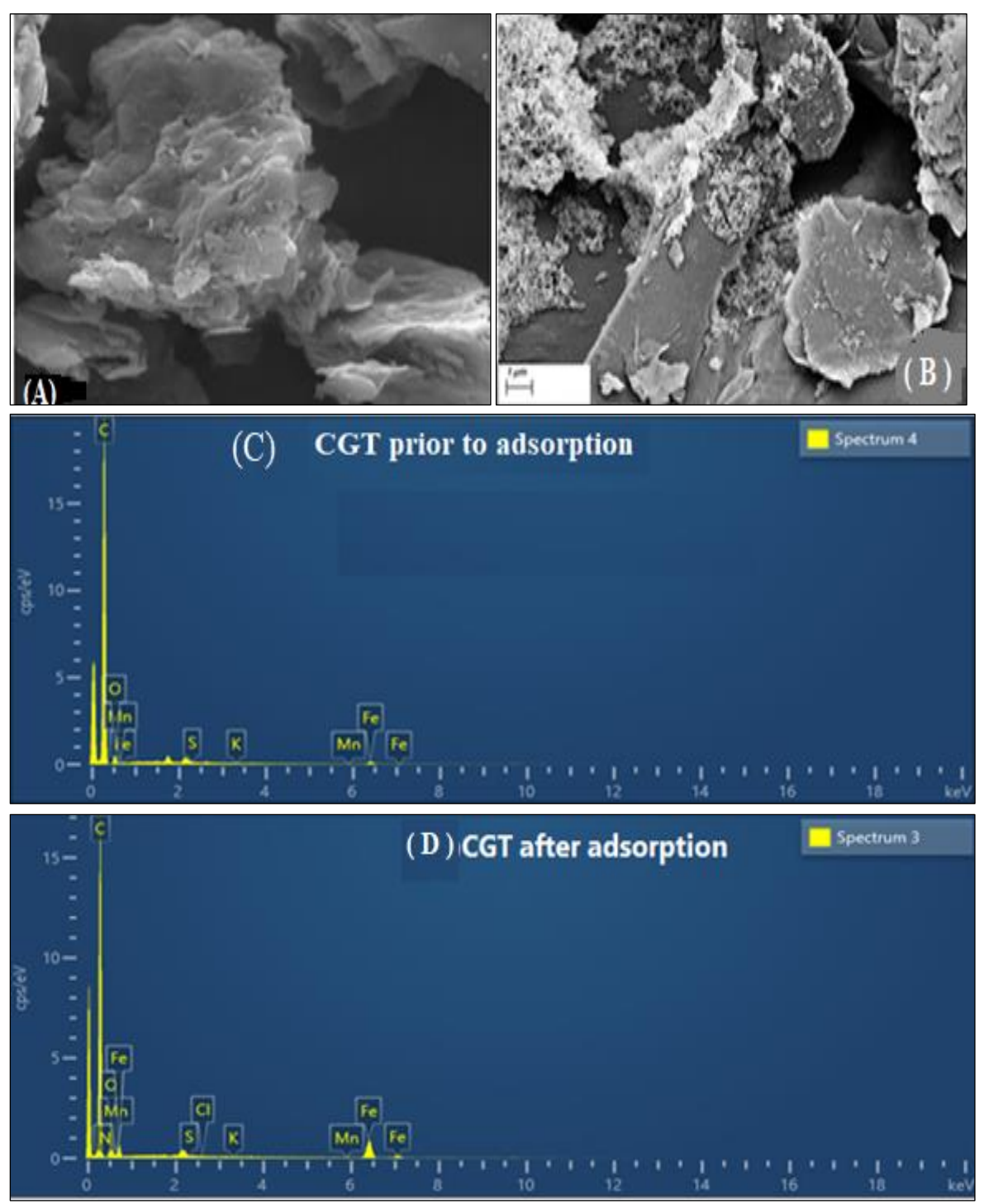


Figure 4. SEM images of CGT adsorbent: **A**- prior to and **B**- after adsorption of JG dye, **C**- and **D**- EDX for CGT prior to and after adsorption JG dye.

3.1.3. The FT-IR

The infrared spectrograms of CGT before and after the adsorption of JG dye are presented in **Figure 5**. As shown in **Figure 5A**, CGT exhibits no discernible signals, likely due to the weak electric dipole induced by the minimal charge difference between sp² carbon atoms.

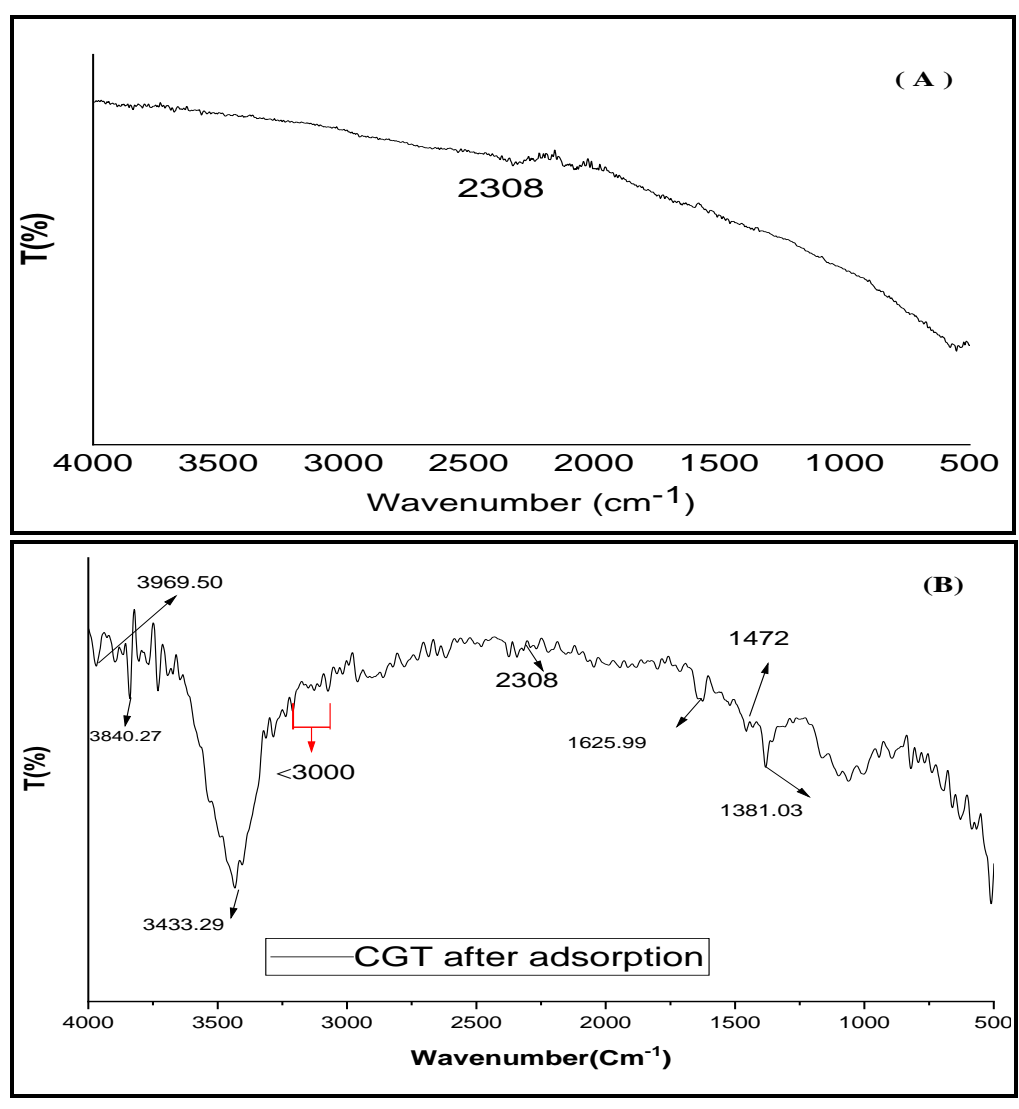


Figure 5. FT-IR spectrum of CGT (A) before adsorption (B) after adsorption.

3.2. Adsorption optimization

Since the amount of adsorbent significantly affects adsorption efficiency, the removal percentage (R%) of JG dye as a function of adsorbent weight was examined. **Figure 6** illustrates the relationship between R% and the adsorbent weight of CGT. The results show that as the CGT weight rises, the percentage removal of JG also rises. This is credited to the increased surface area of CGT, which provides additional adsorption sites.

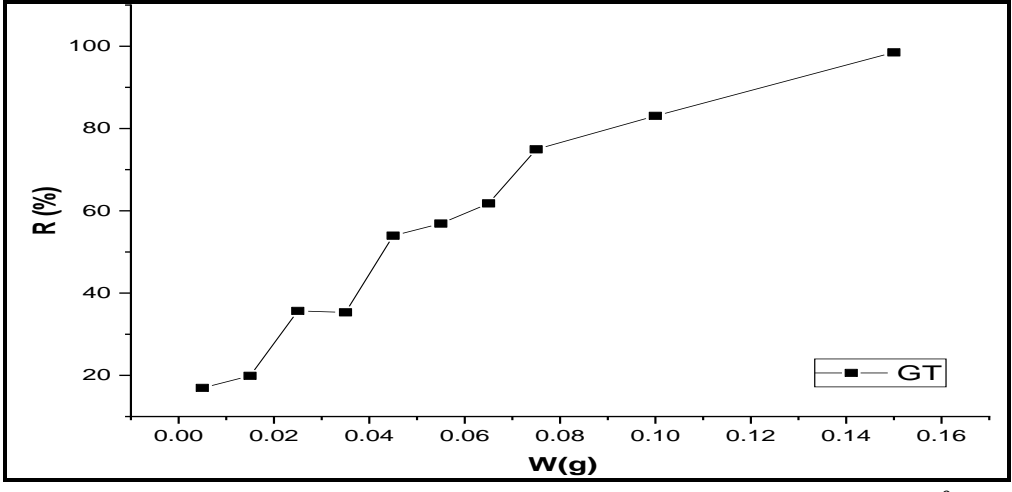


Figure 6. Percentage removal of CGT adsorbent for JG dye vs w (g) of adsorbent at 25 °C.

The 0.15 g of CGT resulted in a maximum removal efficiency of 98.49% for JG dye at 25°C. The relationship between contact time and removal rate is shown in **Figure 7**. The outcomes indicate that the greatest dye removal rate of 98% was accomplished after 45 minutes. The equilibrium reached at this point suggests that the active sites on the CGT were fully occupied. Additionally, the magnitude of JG uptaken on the CGT at time $(q_t, mg/g)$ was graphed versus time at different T as depicted in **Figure 8**.

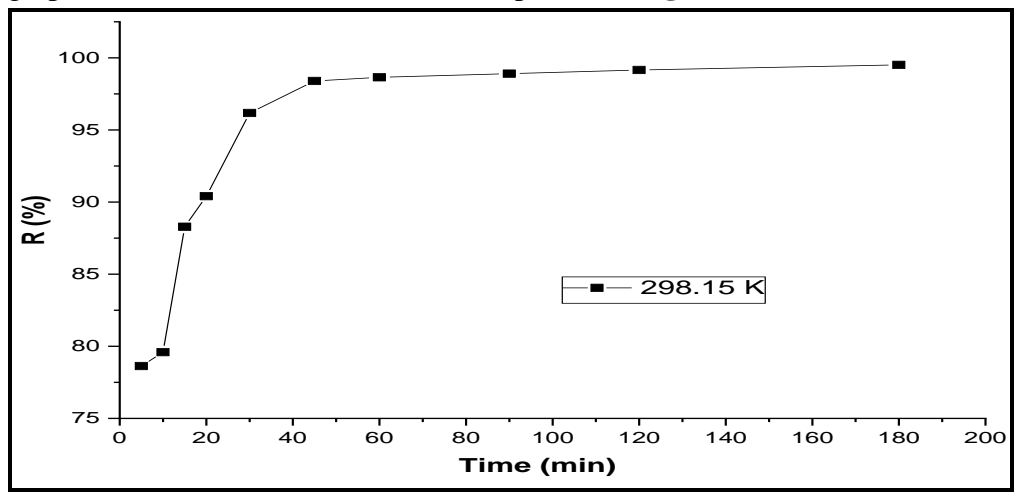


Figure 7. The R% of CGT adsorbent for JG dye vs time(min) at 25 °C.

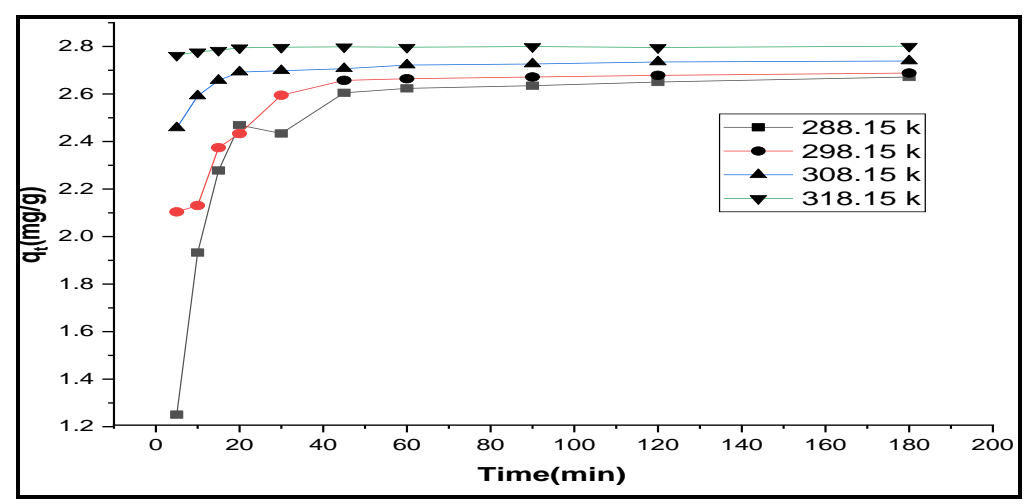


Figure 8. The q_t (mg/g) of JG on CGT vs time (min) at different T.

3.2.1. Impact of temperature on the efficiency of adsorption

The impact of T on the efficiency of adsorption is revealed in **Figure 9**.

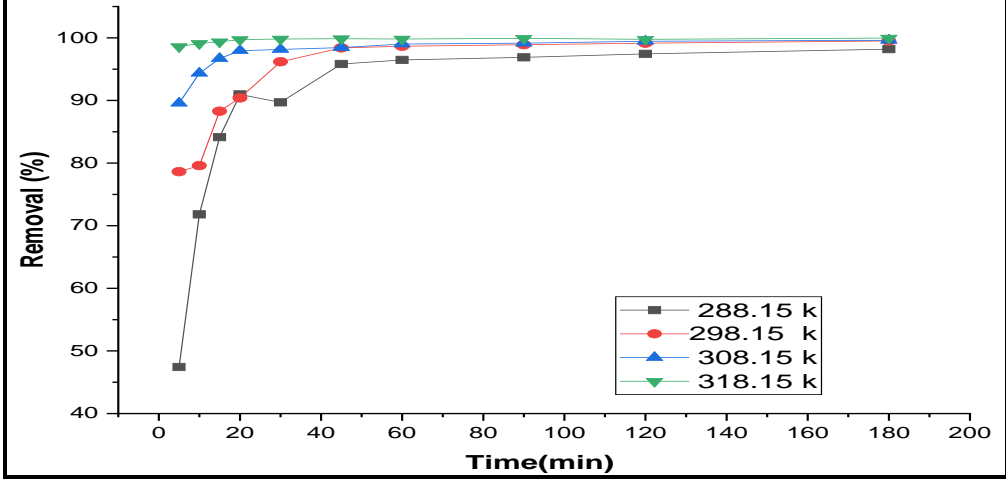


Figure 9. The R% of CGT adsorbent for JG dye versus different T.

3.2.2 Kinetic study of adsorption

The PFO equation, as proposed by Lagergren (17), can be given as **Equation 5**.

$$\operatorname{Ln}\left(q_{e}-q_{t}\right)=\ln q_{e}-\left(\mathbf{k}_{1}\right)t\tag{5}$$

By graphing ln(qe - qt) against time t (min), the slope and intercept of the plot were exploited for determining the rate constant k_1 (min⁻¹) and the adsorption capacity at equilibrium q_e (mg/g). The adsorption capacity at a given time is represented by q_t . The linear expression of the pseudo-second-order model (PSO) model, as presented by Ho and McKay (18), is given by the **Equation 6**.

$$\frac{t}{q_t} = \frac{1}{k_2 q_e^2} + \frac{t}{q_e} \tag{6}$$

The intercept and slope of the graph of (t/q_t) against time t can be utilized to evaluate the equilibrium adsorption capacity q_e (mg/g) and the rate constant of adsorption k_2 (g/mg.min), respectively. **Table 1** presents the correlation coefficient R^2 , rate constants k_1 and k_2 , and equilibrium adsorption capacity q_e of JG at various T as determined from the corresponding equations. The value of the PFO coefficient determination (R^2) at different T is relatively low: 0.8383, 0.8636, 0.8936, and 0.4495. Furthermore, the discrepancy between the theoretical (cal) and the experimental (exp) qe values at all T suggests that PFO kinetics do not describe JG dye adsorption. The compatibility between the experimental and theoretical (q_e) magnitudes with $R^2 \le 1$ in the PSO kinetic model makes the PSO model more applicable to the mechanism of JG dye adsorption on the CGT surface at different T.

Table 1. Adsorption JG on CGT using PFO and PSO kinetic model data.

T/K	PFO				PSO			
	\mathbf{k}_1	$q_{e(exp)}$	$\mathbf{q}_{e(cal)}$	\mathbb{R}^2	\mathbf{k}_2	$\mathbf{q}_{\mathrm{e}(\mathrm{exp})}$	$\mathbf{q}_{e(cal)}$	\mathbb{R}^2
	min ⁻¹	(mg/g)	(mg/g)		(gm/mg.min)	(mg/g)	(mg/g)	
288.15	0.0334	2.749469	0.669181	0.8383	0.3561	2.749469	2.8082	0.9997
298.15	0.0372	2.78627	0.449868	0.8636	0.201574	2.78627	2.818489	0.9999
308.15	0.0307	2.789101	0.14921	0.8936	0.652739	2.789101	2.797203	1
318.15	0.0181	2.799009	0.015719	0.4495	4.835731	2.799009	2.798769	1

To pinpoint the step that limits the rate of adsorption, the Weber and Morris model can be applied (19,20) using the **Equation 7**.

$$q_t = k_d \cdot t^{1/2} + C \tag{7}$$

Where C (mg/g) and k_d (g/mg.min^{1/2}) are the thickness of the boundary layer and rate constant of the intraparticle diffusion, respectively, t is the time (min). C and k_d can be determined from the intercept and slope, respectively, by plotting the relationship between q_t and $t^{1/2}$ (**Figure 10**). The intraparticle diffusion analysis of JG adsorption onto CGT reveals two distinct stages in the entire adsorption phenomenon. The preliminary stage corresponds to the diffusion of JG motes into the active sites, and the first-stage intraparticle diffusion rate constant k_1 is relatively high. In the second stage (equilibrium phase), the intraparticle diffusion rate begins to slow down as the dye content in the solution becomes very low and the maximum sorption ability is reached. The values of k_2 in this plateau region are minimal. The values of the intraparticle diffusion rate constants k_1 and k_2 are listed in **Table 2**.

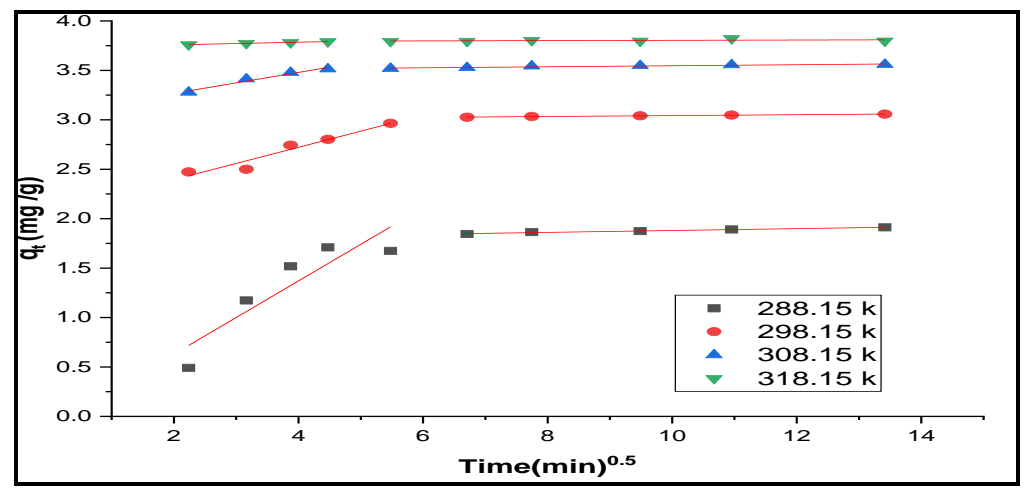


Figure 10. Weber and Morris model plot at different T for removing JG dye by CGT.

Table 2. The variables of Weber& Morris intraparticle diffusion of adsorption JG dye on CGT surface at different T.

Kinetics Parameter	rs			
Segment 1	288.159	298.15	308.15	318.15
C	0.72816	1.79733	2.72461	2.73085
\mathbf{k}_{1}	0.37006	0.16337	0.00519	0.01356
\mathbb{R}^2	0.81644	0.93906	0.89626	0.99296
Segment 2				
C	2.62316	2.72589	2.28631	2.78965
k ₂	0.0095	0.00455	0.10576	0.00145

3.2.3. Determination of activation energy (E_a) and thermodynamic functions

The Ea for the removal of JG dye by the CGT adsorbent and thermodynamic functions was explained by the Arrhenius equation (21).

$$Ln K_2 = LnA - \frac{E_a}{RT} \tag{8}$$

Where k (g.mg⁻¹.min⁻¹) represents the rate constant, which is computed according to the PSO model, R (8.314 J/K.mol), E_a (J/mol), T (K), and A represent the adsorption rate constant, the universal gas constant, the activation energy, the temperature, and the Arrhenius coefficient, respectively. The E_a value can be computed from the slope of the plot of lnk against 1/T using the regression equation (Y= -11452 X + 37.158 with R^2 = 0.9290) (22).

To include additional understanding of the reaction mechanism, the thermodynamic functions of activation of enthalpy (ΔH^*), free energy (ΔG^*), and entropy (ΔS^*) were calculated using the Eyring relation (23):

$$ln\frac{k_2}{T} = \ln\frac{k_B}{h} + \frac{\Delta S^*}{R} - \frac{\Delta H^*}{RT}$$
(9)

Where K_B , k_2 , and h stand for the Boltzmann constant, the rate constant of PSO, and the Planck constant, respectively. Plotting produced a straight line. The ΔS^* and ΔH^* were obtained from using the intercept and the slope of plotting $ln(k_2/T)$ against 1/T. The values of ΔH^* and ΔS^* were used to calculate the value of ΔG^* of activation using the relation below (24). **Table 3** contains the values of ΔG^* , ΔS^* and ΔH^* .

$$\Delta G^* = \Delta H^* - T \Delta S^* \tag{10}$$

Table 3. Evaluate the thermodynamic functions of activation for the adsorption of dye JG on the surface of CGT at different T.

T (k)	$\Delta \mathbf{G}^* (\mathbf{KJ.mol}^{-1})$	$\Delta H^* (KJ.mol^{-1})$	$\Delta S^* (J.mol^{-1} K^{-1})$
288.15	76.686		
298.15	76.130	92.701	55.579
308.15	75.574		
318.15	75.018		

3.2.4 The adsorption isotherms

The Langmuir model hypothesizes that the adsorbent surface consists of active sites with equal energy, where each site adsorbs one molecule of the adsorbate without interacting with molecules on adjacent sites, implying that the adsorption occurs in a monolayer. The straight-line version of this model was expressed by the **Equation 11**, as shown below (25):

$$\frac{c_e}{q_e} = \frac{1}{q_{\text{max}} \cdot k_L} + \frac{c_e}{q_{\text{max}}} \tag{11}$$

Where q_e (mg/g) and C_e (mg/L) are the amount and the concentration of adsorbate at equilibrium, respectively, q_{max} (mg/g) is the maximum adsorption ability, and K_L (L/mg) is the Langmuir constant. The magnitudes of q_{max} and K_L were derived from the slope and intercept of the C_e/q_e vs. The C_e plot was shown in **Table 4**. The dimensionless separation factor (R_L) is a critical Langmuir parameter (26) and can be computed from the highest concentration of JG dye C° (mg/L) using the **Equation 12**.

$$R_{L} = \frac{1}{1 + K_{L}C^{\circ}} \tag{12}$$

The isotherm shape can be characterized by the value of the separation factor R_L . The calculated data is presented in **Table 4**. The Freundlich isotherm was represented by the following formula (27):

$$\ln q_e = \ln K_F + \frac{1}{n} \ln c_e \tag{13}$$

Where C_e (mg/L), q_e (mg/g), K_F (L/mg), and n are the concentration of the adsorbed JG dye at equilibrium, adsorption capacity, Freundlich constant, and intensity, respectively, the intercept and slope from the $ln(q_e)$ vs. $ln(C_e)$ plot allow for the estimation of K_F and 1/n, respectively. **Table 4** shows the parameters of the Freundlich model. The n values are greater than unity, suggesting that the adsorption of JG dye on CGT is favorable at all T examined (28), according to the **Equation 14**.

$$q_e = BLnK_T + BLnC_e (14)$$

The constant B and binding constant K_T (L/g) might be determined from the intercept and slope of the plot of q_e versus ln Ce. The **Equation 15** describes how the B constant is related to the heat of adsorption:

$$B = \frac{RT}{h} \tag{15}$$

The Temkin constant b (J/mol) is linked to the heat of adsorption (29). **Table 4** presents the computed parameters for the Langmuir, Temkin, and Freundlich models at different T. The practical data presented in **Table 4** are more consistent with the Langmuir isotherm as indicated by the high $R^2 = 0.998$, compared to the other models.

Table 4. Isotherm parameters for Langmuir, Temkin, and Freundlich at various temperature conditions.

Isotherm		Te		
Parameters	288.15	298.15	308. 15	318.15
Langmuir				
q_{m} (mg. g^{-1})	3.808073	4.116921	4.246285	4.545455
$K_L(L.mg^{-1})$	3.370988	1.224294	2.148723	5.759162
\mathbb{R}^2	0.9993	0.9913	0.9937	0.9983
$R_{ m L}$	0.0036	0.01	0.0057	0.0021
Freundlich				
$K_F (L. mg^{-1})$	2.940854	2.696622	2.961512	3.54203
n	11.13586	7.304602	7.53012	8.920607
\mathbb{R}^2	0.7782	0.8298	0.7894	0.7626
Temkin				
B_T (KJ. mol^{-1})	8.552942	5.732699	5.829258	6.72378
K_T (L. mg^{-1})	41614.39	533.9467	936.0213	10032.42
R^2	0.8166	0.8359	0.8226	0.8253

4. Disussion

4.1. Identification of commercial graphite

4.1.1. The X- ray diffraction analysis

The diffraction pattern of CGT exhibits a strong peak at $2\theta = 26.57^{\circ}$ corresponding to a distance between the planes (d) of 0.3351 nm (JCPDS no. 41-1487) and the (002) reflection planes (30). Based on **Equations 3** and **4**, the presence of 78.84 layers in CGT confirms that the graphite is composed of nanoplate structures (31).

4.1.2. The SEM and EDX

The SEM image shows a clear lamellar structure of natural graphite with particles appearing as overlapping sheets with thin and irregular edges. This morphology is consistent with the properties of flaky graphite (FG), which has a relatively regular crystal structure that contributes to its layered appearance (32). After adsorption, the CGT sample showed the aggregation of JG particles on its surface. Atomic imaging shows peaks that correspond to nitrogen (N), carbon (C), and chlorine (Cl), which are linked to the JG dye, as well as carbon (C) and oxygen (O) from the CGT. Traces of heteroatoms such as sulfur (S), manganese (Mn), and iron (Fe) were also detected, likely as contaminants from the manufacturing process. The presence of these functional groups can provide chemical binding sites for the JG dye (33).

4.1.3. The FT-IR

The absorption peak at 2308 cm⁻¹ is attributed to the asymmetric (asym.) stretching of CO₂ (34). After adsorption of JG dye, the spectrum of CGT shows distinctive peaks at 1625 cm⁻¹ and 1472 cm⁻¹ relating to the C=C group. Furthermore, the stretching vibration of the azo groups is observed near the double bond stretching region. The region above 3000 cm⁻¹ corresponds to the stretching mode of the C-H aromatic group. The absorption band at 1381 cm⁻¹ is associated with the stretching mode of C-N (34). These results suggest the involvement of strong electrostatic interactions and chemical bonding between the functional points on the CGT surface and the JG dye, which give rise to changes in the infrared spectra of the CGT surface moieties.

4.2. Adsorption optimization

The rapid adsorption process in the initial minutes can be ascribed to the initially unoccupied adsorption sites. Over time, the rate of adsorption slowed until it reached equilibrium at 45 minutes as the JG dye molecules transferred to the surface of CGT (35).

4.2.1. Impact of temperature on the efficiency of adsorption

To examine the influence of temperature on the adsorption of JG dye onto the CGT surface, the adsorption system was conducted at various T. The findings showed that adsorption efficiency increased with rising temperature, with the highest removal rate of 99.96% achieved at 45 °C. This suggests that the adsorption phenomenon is endothermic enclosed by the specified temperature interval.

4.2.2 Kinetic study of adsorption

The adsorption dynamics is a key factor in determining the effectiveness of adsorption diffusion. To estimate the adsorption kinetics, several kinetic approaches were employed to the experimental results incorporating intraparticle diffusion, pseudo-first and second order (PFO and PSO) models at different T according to the linear expression of the PSO model by Ho and McKay. To pinpoint the step that limits the rate of adsorption, the Weber and Morris model was used. Additionally, the plot does not intersect the origin, which indicates that intraparticle diffusion is not the sole determinant of the rate and that alternative kinetic approaches may also govern the adsorption of JG onto CGT (36).

4.2.3. Determination of activation energy (Ea) and thermodynamic functions

The Ea for the removal of JG dye by the CGT adsorbent was computed with the Arrhenius equation. The ΔH^* , ΔG^* , and ΔS^* were calculated using the Eyring relation. Values of ΔH^* and ΔS^* were used to calculate the value of ΔG^* of activation. The value of ΔH^* for the adsorption of JG onto the CGT surface is 92.701. This value falls within the range of 40 KJ.mol⁻¹ and 120 KJ.mol⁻¹, indicating the adsorption process is chemisorption. The positive sign of this value further confirms the endothermic nature of JG adsorption. This outcome is in complete agreement with the kinetics data and the Ea value. The values of ΔG^* are positive at all T studied, indicating that the adsorption process requires energy to convert reactants (dye molecules in solution) into products (dye molecules on the surface). Additionally, the removal of JG dye onto CGT shows a positive value of ΔS^* due to an increase in disorder at the interface (solid-solution) (37).

4.2.4 The adsorption isotherms

An isotherm of adsorption study delivers valuable insights into the adsorption process, including its conditions, the concentration of the dye (adsorbate), and the adsorption capacity of the CGT (adsorbent) at equilibrium. In this study, various isotherm models were implemented on the experimental data at different T and the straight-line version of this model was calculated and the R_L was calculated. Multilayer adsorption involving a varied energy distribution of active sites on the adsorbent is represented by the Freundlich isotherm. The Temkin isotherm considers the influence of non-direct interactions between adsorbate-adsorbent entities on adsorption. Due to these interactions, the model predicts that the heat of adsorption as a function of temperature of all the molecules in the layer will decrease linearly rather than logarithmically (38). Also, the adsorption heat was calculated. Additionally, the R_L value ranging from 0 to 1 indicates that the adsorption process was favorable for JG dye. Alternatively, the minor R^2 values for the Temkin and the Freundlich isotherms suggest that these models did not fit the experimental data as well (39).

5. Conclusion

This study evidences the efficiency of CGT as an adsorbent for the removal of JG dye from aqueous solutions. The obtained data show that the amount of JG dye (q_e in mg/g) increases with the weight of the CGT adsorbent. Kinetic analysis reveals that the removal mechanism is more congruent with the PSO model ($R^2 \le 1$). The adsorption data isotherms fit the Langmuir

model. The adsorption is endothermic and non-spontaneous, with an increase in randomness as evidenced by the thermodynamic analysis. The adsorption efficiency of the CGT adsorbent demonstrated the highest removal rate of 99.96% at the highest temperature. This indicates that the surface is highly effective as an adsorbent for removing JG dye within the temperature range studied.

Acknowledgment

The authors express their gratitude to the Department of Chemistry at the University of Baghdad, College of Education for Pure Science (Ibn Al-Haitham), for their assistance.

Conflict of Interest

The authors declare that they have no conflicts of interest.

Funding

There is no financial support.

Ethical Clearance

This study was approved by the University of Baghdad, College of Education for Pure Science (Ibn Al-Haitham).

References

- Zainurin SN, Wan Ismail WZ, Mahamud SNI, Ismail I, Jamaludin J, Ariffin KNZ, Wan Ahmad Kamil WM. Advancements in monitoring water quality based on various sensing methods: A systematic review. Int J Environ Res Public Health. 2022; 19(21):14080. https://doi.org/10.3390/ijerph192114080.
- 2. Ardila-Leal LD, Poutou-Piñales RA, Pedroza-Rodríguez AM, Quevedo-Hidalgo BE. A brief history of colour, the environmental impact of synthetic dyes and removal by using laccases. Molecules. 2021; 26(13): 3813. https://doi.org/10.3390/molecules26133813.
- 3. Nishat A, Yusuf M, Qadir A, Ezaier Y, Vambol V, Khan MI Sana Ben Moussa, Hesam Kamyab, Satbir S, Sehgal, Chander Prakash, Hsi-Hsien Yang, Hussameldin Ibrahim, Sayed M. Eldin. Wastewater treatment: A short assessment on available techniques. Alexandria Eng J. 2023; 76:505–516. https://doi.org/10.1016/j.aej.2023.06.054.
- 4. Khan MI, Shanableh A, Nasir N, Shahida S. Adsorptive removal of methyl orange from wastewaters by the commercial anion exchange membrane EPTAC. Desalin Water Treat. 2021; 234:245–254. https://doi.org/10.5004/dwt.2021.27619.
- 5. Farhood AS, Ali LAM, Majeed AS, Taha DN. Batch adsorption technique for the removal of Janus Green B dye from industrial waste water by using walnut kernel shell as adsorbent. Ann Rom Soc Cell Biol. 2021; 25(7):154–168. http://annalsofrscb.ro/index.php/journal/article/view/9497.
- 6. Singh NB, Nagpal G, Agrawal S. Water purification by using adsorbents: a review. Environ Technol Innov. 2018; 11(4):187–240. https://doi.org/10.1016/j.eti.2018.05.006.
- 7. Pierson HO. Handbook of carbon, graphite, diamonds and fullerenes: processing, properties and applications. William Andrew; 2012.
- 8. Yaya A, Agyei-Tuffour B, Dodoo-Arhin D, Nyankson E, Annan E, Konadu DS, Sinayobye E, Baryeh EA, Ewels CP. Layered nanomaterials-a review. Glob J Eng Des Technol. 2012; 1(2):32–41. https://doi.org/10.4236/csta.2024.121001.
- 9. Ivancev-Tumbas I, Landwehrkamp L, Hobby R, Vernillo M, Panglisch S. Adsorption of organic pollutants from the aqueous phase using graphite as a model adsorbent. Adsorpt Sci Technol. 2020; 38(7–8):286–303. https://doi.org/10.1177/0263617420945847.
- 10. Abdul Halim H, Ali Bashah NA, Nor NM. Graphite as apotential adsorbent for ammonium ions removal. Esteem Acad J. 2022; 18:31-40. https://ir.uitm.edu.my/id/eprint/68047.

- 11.Gawad SAA, Ghazy R, Mansour S, Ahmed H, Ghazy AR. Photo-physical characteristics of Janus green b in different solvents and its interaction mechanism with silver nanoparticles. J Fluoresc. 2024; 35(5): 3363-3376. https://doi.org/10.1007/s10895-024-03723-8.
- 12.Ali NS, Jabbar NM, Alardhi SM, Majdi HS, Albayati TM. Adsorption of methyl violet dye onto a prepared bio-adsorbent from date seeds: Isotherm, kinetics, and thermodynamic studies. Heliyon. 2022; 8(8):e10276. https://doi.org/10.1016/j.heliyon.2022.e10276.
- 13.Ali OS, AL-Mammar D E. Adsorption of the color pollutant onto NiO nanoparticles prepared by a new green method. Iraqi J Sci. 2024; 65(4):1824-1838. https://doi.org/10.24996/ijs.2024.65.4.4.
- 14. Sultan MS, Radi MF, Jasim AA, Tahir JS, Abdul Ghani LH, Maryoosh AA, Abdul abass DA. Removing of hexavalent chromium from aqueous solutions using dried yogurt, and studying isotherm, kinetic and thermodynamic parameters. Baghdad Sci J. 2019; 16(3):603-609. http://dx.doi.org/10.21123/bsj.2019.16.3.0603.
- 15. Farhan AM, Zaghair AM, Abdullah HI. Adsorption study of rhodamine—b dye on plant (*Citrus* Leaves). Baghdad Sci J. 2022; 19(4):838-847. https://doi.org/10.21123/bsj.2022.19.4.0838.
- 16.Bannov AG, Ukhina AV, Maksimovskii EA, Prosanov IY, Shestakov AA, Lapekin NI, Lazarenko NS, Kurmashov PB, Popov MV. Highly porous expanded graphite: thermal shock vs. programmable heating. Materials (Basel). 2021; 14(24):7687. https://doi.org/10.3390/ma14247687.
- 17.AL-Shammari NH, AL-Mammar DE. Adsorption of biebrich scarlet dye into remains chromium and vegetable tanned leather as adsorbents. Iraqi J Sci. 2022; 63(7):2814-2826. https://doi.org/10.24996/ijs.2022.63.7.6.
- 18.Al-Mammar DE. Characteristics of azo-dye onto surfactant modified chromium contained leather waste. IOSR-JAC. 2014; 7(2):83-92. https://doi.org/10.9790/5736-07218392.
- 19.Jawad AH, Saber SEM, Abdulhameed AS, Farhan AM, ALOthman ZA, Wilson LD. Characterization and applicability of the natural Iraqi bentonite clay for toxic cationic dye removal: Adsorption kinetic and isotherm study. J King Saud Univ. 2023; 35(5):102630. https://doi.org/10.1016/j.jksus.2023.102630.
- 20. Abbas A, Merza S. Preparation and characterization of graphene oxide–attapulgite composite and its use in kinetic study of alizarin dye adsorption from aqueous media. Egypt J Chem. 2020; 63(2):561–672. https://doi.org/10.21608/ejchem.2019.15600.1946.
- 21. Najm ZA, Atiya MA, Hassan KA. Adsorption and photocatalytic of biosynthesis zinc ferrite nanoparticles for removing acid black 210 dye from aqueous medium. Baghdad Sci J. 2025; 22(3): 756-770. https://doi.org/10.21123/bsj.2024.9359.
- 22.Yusof AM, Malek NANN. Removal of Cr (VI) and As (V) from aqueous solutions by HDTMA-modified zeolite Y. J Hazard Mater. 2009; 162(2–3):1019–1024. https://doi.org/10.1016/j.jhazmat.2008.05.134.
- 23.Bengar S A,Zanjanchi M A,Sohrabnezhad S. Adsorptive characteristics and performance of template-containing MCM-41 for removal of sodium dodecylbenzene sulfonate from aqueous solutions. Desalin Water Treat. 2021; 212:415-427. https://doi.org/10.5004/dwt.2021.26601.
- 24.Doğan M, Hamdi M, Alkan M. Adsorption kinetics of maxilon yellow 4GL and maxilon red GRL dyes on kaolinite. HAZMAT. 2009; 165(1-3):1142-1151. https://doi.org/10.1016/j.jhazmat.2008.10.101.
- 25.Mpelane S, Mketo N, Bingwa N, Nomngongo PN. Synthesis of mesoporous iron oxide nanoparticles for adsorptive removal of levofloxacin from aqueous solutions: Kinetics, isotherms, thermodynamics and mechanism. Alexandria Eng J. 2022; 61(11):8457–8468. https://doi.org/10.1016/j.aej.2022.02.014.
- 26. Abduljabar MA, Merza SH. Graphene oxide decorated with nickel cobaltite nanoparticles as an adsorbent for cationic methyl green dye: kinetic, isotherm, and thermodynamic studies. Baghdad Sci J. 2024; 21(9):2853-2865. https://doi.org/10.21123/bsj.2024.8742.
- 27. Nandiyanto ABD, Hofifah SN, Inayah HT, Putri SR, Apriliani SS, Anggraeni S, Usdiyana D, Rahmat A. Adsorption isotherm of carbon microparticles prepared from pumpkin (Cucurbita maxima) seeds for dye removal. Iraqi J Sci. 2021; 62(5):1404–1414. https://doi.org/10.24996/ijs.2021.62.5.2.

- 28.Khan NA, Shaheen S, Najam T, Shah SSA, Javed MS, Nazir MA, Ejaz Hussain, Shaheen A, Hussain Sh, Ashfaq M. Efficient removal of norfloxacin by MOF@ GO composite: isothermal, kinetic, statistical, and mechanistic study. Toxin Rev. 2020; 40(4):915–927. https://doi.org/10.1080/15569543.2020.1801750.
- 29.Kadhim HH, Saleh KA. Removing of copper ions from industrial wastewater using graphene oxide/ chitosan nanocomposite. Iraqi J Sci. 2022; 63(5):1894–18908. https://doi.org/10.24996/ijs.2022.63.5.4.
- 30.Heo YJ. Control of interlayer spacing of expanded graphite for improved hydrogen storage capacity. Carbon Lett. 2018; 27(1):117–120. https://doi.org/10.5714/CL.2018.27.117.
- 31.Bianco A, Cheng HM, Enoki T, Gogotsi Y, Hurt RH, Koratkar N, Kyotani, Takashi, Marc M, Chong Rae P, Juan T, Jin Z. All in the graphene family–A recommended nomenclature for two-dimensional carbon materials. Carbon. Elsevier. 2013; 65:1–6. https://doi.org/10.1016/j.carbon.2013.08.038.
- 32.Peng W, Hon G, Huang Y, Cao Y, Song S. Insight the effect of crystallinity of natural graphite on the electrochemical performance of reduced graphite oxide. Results Phys. 2018; 11:131-37. https://doi.org/10.1016/j.rinp.2018.08.055.
- 33.Oliveira LS, Alba JFG, Silva VL, Ribeiro RT, Falcao EHL, Navarro M. The effect of surface functional groups on the performance of graphite powders used as electrodes. J Electroanal Chem. 2018; 818:106–113. https://doi.org/10.1016/j.jelechem.2018.04.022.
- 34.Ruiz S, Tamayo JA, Ospina JD, Navia Porras DP, Valencia Zapata ME, Hernandez JHM, Valencia CH, Zuluaga F, Grande Tovar CD. Antimicrobial films based on nanocomposites of chitosan/poly(vinyl alcohol)/graphene oxide for biomedical applications. Biomolecules. 2019; 9(3):109. https://doi.org/10.3390/biom9030109.
- 35.Coates J. Interpretation of infrared spectra, a practical approach. Encycl Anal Chem. 2006; 12:10815. https://doi.org/10.1002/9780470027318.a5606.
- 36.Basu S, Ghosh G, Saha S. Adsorption characteristics of phosphoric acid induced activation of biocarbon: Equilibrium, kinetics, thermodynamics and batch adsorber design. Process Saf Environ Prot. 2018; 117:125-142. https://doi.org/10.1016/j.psep.2018.04.015.
- 37.Al-Khalisy RS, Al-Haidary AMA, Al-Dujaili AH. Aqueous phase adsorption of cephalexin onto bentonite and activated carbon. Sep Sci Technol. 2010; 45(9):1286–1294. https://doi.org/10.1080/01496391003689017.
- 38. Aljamali NM, Aldujaili RA, Alfatlawi IO. Physical and chemical adsorption and its applications. IJTCK. 2021; 7(2):1-8. https://doi.org/10.37628/IJTCK.
- 39. Abbas M, Trari M. Kinetic, equilibrium and thermodynamic study on the removal of congo red from aqueous solutions by adsorption onto apricot stone. Process Saf Environ Prot. 2015; 98(6):424–436. https://doi.org/10.1016/j.psep.2015.09.015.